Simulation of Double-Front Detonation of Suspended Mixed Cyclotrimethylenetrinitramine and Aluminum Dust in Air

Wen-Tao Zan(昝文涛)[1,2], He-Fei Dong(董贺飞)[2], Tao Hong(洪滔)[2**]

[1]*School of Mechatronical Engineering, Beijing Institute of Technology, Beijing 100081*
[2]*Institute of Applied Physics and Computational Mathematics, Beijing 100094*

(Received 29 November 2016)

The two-phase detonation of suspended mixed cyclotrimethylenetrinitramine (i.e., RDX) and aluminum dust in air is simulated with a two-phase flow model. The parameters of the mixed RDX-Al dust detonation wave are obtained. The double-front detonation and steady state of detonation wave of the mixed dust are analyzed. For the dust mixed RDX with density of 0.565 kg/m^3 and radius of 10 μm as well as aluminum with density of 0.145 kg/m^3 and radius of 4 μm, the detonation wave will reach a steady state at 23 m. The effects of the size of aluminum on the detonation are analyzed. For constant radius of RDX particles with radius of 10 μm, as the radius of aluminum particles is larger than 2.0 μm, the double-front detonation can be observed due to the different ignition distances and reaction rates of RDX and aluminum particles. As the radius of aluminum particles is larger, the velocity, pressure and temperature of detonation wave will be slower. The pressure at the Chapman–Jouguet (CJ) point also becomes lower. Comparing the detonation with single RDX dust, the pressure and temperature in the flow field of detonation of mixed dust are higher.

PACS: 47.40.Rs, 47.61.Jd DOI: 10.1088/0256-307X/34/7/074701

The research of dust detonation is very important due to its applications in industrial safety policies and military. Most research focuses on the single dust such as coal dust, cornstarch dust and aluminum dust. The detonation of mixed dusts is not studied as much as the single dust detonation. Hong *et al.*[1,2] studied the parameters of detonation wave of suspended aluminum dust and simulated the detonation of RDX dust with the MacCormack method. Veyssiere *et al.*[3] studied the formation of cellular detonation of aluminum particles by simplified diffusion combustion models. The two-step model was used by Briand *et al.*[4] to simulate the detonation cellular structure later. Teng and Jiang[5] studied the effects of product phases and the choice of heat release of Al dust detonations. Khasainov and Khasainov,[6,7] and Uphoff and Hanel [8] discussed the pseudo-gas detonation, the single-front detonation and the double-front detonation of steady two-phase detonation in mixed gas and suspended particles. The pseudo-gas detonation wave is supported by energy released by gas. The particles and gas both release energy in single-front detonation. The front wave of double-front detonation is supported by energy of gas and the second wave is supported by energy of solid particles. Michael[9] studied the non-ideal detonation in ammonium perchlorate/aluminum mixtures with theoretical analysis. The detonation of ammonium nitrate and aluminum dust mixtures are simulated by Khasainov and Ermolaev.[10] Hong *et al.*[11] simulated the detonation in suspended mixed RDX and aluminum dusts. The parameters of detonation waves of mixture dusts and single dust were discussed.

In this Letter, we investigate the double-front detonation of suspended mixed RDX and Al dust in air with the two-phase model and the space-time conservation element and solution element (CE/SE) method,[12–16] and discuss the effects of the radius of particles on the detonation wave and the characteristics of the double-front detonation.

The two-phase flow model is used in numerical simulation. It is assumed that the particles are spherical, the initial diameters of particles are the same, also the temperatures inside a particle are the same. Because particles in the model are sparse, the interaction and pressure of particles are ignored. The energy of chemical reaction is absorbed by gas. Heat conduction between gas and wall is ignored. The governing equations for the mixtures are as follows:[17] For gas

$$\frac{\partial(\rho_1\phi_1)}{\partial t}+\frac{\partial(\rho_1\phi_1 u_1)}{\partial x}+\frac{\partial(\rho_1\phi_1 v_1)}{\partial y}=I_{\mathrm{d2}}+I_{\mathrm{d2a}}, \tag{1}$$

$$\begin{aligned}&\frac{\partial(\rho_1\phi_1 u_1)}{\partial t}+\frac{\partial(\rho_1\phi_1 u_1^2+p)}{\partial x}+\frac{\partial\rho_1\phi_1 u_1 v_1}{\partial y}\\&=I_{\mathrm{d2}}u_2-F_{\mathrm{d2}x}+I_{\mathrm{d2a}}u_{2\mathrm{a}}-F_{\mathrm{d2a}x},\end{aligned} \tag{2}$$

$$\begin{aligned}&\frac{\partial(\rho_1\phi_1 v_1)}{\partial t}+\frac{\partial(\rho_1\phi_1 u_1 v_1)}{\partial x}+\frac{\partial(\rho_1\phi_1 v_1^2+p)}{\partial y}\\&=I_{\mathrm{d2}}v_2-F_{\mathrm{d2}y}+I_{\mathrm{d2a}}v_{2\mathrm{a}}-F_{\mathrm{d2a}y},\end{aligned} \tag{3}$$

$$\begin{aligned}&\frac{\partial\rho_1\phi_1(e_1+0.5(u_1^2+v_1^2))}{\partial t}\\&\quad+\frac{\partial\phi_1 u_1(\rho_1 e_1+0.5\rho_1(u_1^2+v_1^2)+p)}{\partial x}\\&\quad+\frac{\partial\phi_1 v_1(\rho_1 e_1+0.5\rho_1(u_1^2+v_1^2)+p)}{\partial y}\\&=-Q_{\mathrm{d2}}+I_{\mathrm{d2}}(e_2+0.5(u_2^2+v_2^2))\\&\quad+I_{\mathrm{d2}}q_2-F_{\mathrm{d2}x}u_2-F_{\mathrm{d2}y}v_2-Q_{\mathrm{d2a}}\\&\quad+I_{\mathrm{d2a}}(e_{2\mathrm{a}}+0.5(u_{2\mathrm{a}}^2+v_{2\mathrm{a}}^2))+I_{\mathrm{d2a}}q_{2\mathrm{a}}\\&\quad-F_{\mathrm{d2a}x}u_{2\mathrm{a}}-F_{\mathrm{d2a}y}v_{2\mathrm{a}}.\end{aligned} \tag{4}$$

For solid

$$\frac{\partial(\rho_i\phi_i)}{\partial t}+\frac{\partial(\rho_i\phi_i u_i)}{\partial x}+\frac{\partial(\rho_i\phi_i v_i)}{\partial y}=-I_{\mathrm{d}i}, \tag{5}$$

**Corresponding author. Email: hongtao@iapcm.ac.cn
© 2017 Chinese Physical Society and IOP Publishing Ltd

$$\frac{\partial(\rho_i\phi_i u_i)}{\partial t}+\frac{\partial(\rho_i\phi_i u_i^2)}{\partial x}+\frac{\partial(\rho_i\phi_i u_i v_i)}{\partial y} = -I_{\mathrm{d}i}u_i+F_{\mathrm{d}ix}, \tag{6}$$

$$\frac{\partial\rho_i\phi_i v_i}{\partial t}+\frac{\partial\rho_i\phi_i u_i v_i}{\partial x}+\frac{\partial\rho_i\phi_i v_i^2}{\partial y} = -I_{2i}v_i+F_{2iy}, \tag{7}$$

$$\frac{\partial[\rho_i\phi_i(e_i+0.5(u_i^2+v_i^2))]}{\partial t}+\frac{\partial[\rho_i\phi_i u_i(e_i+0.5(u_i^2+v_i^2))]}{\partial x}+\frac{\partial[\rho_i\phi_i v_i(e_i+0.5(u_i^2+v_i^2))]}{\partial y} = Q_{\mathrm{d}i}-I_{\mathrm{d}i}(e_i+0.5(u_i^2+v_i^2))+F_{\mathrm{d}ix}u_i+F_{\mathrm{d}iy}v_i, \tag{8}$$

$$\frac{\partial n_i}{\partial t}+\frac{\partial(nu_i)}{\partial x}+\frac{\partial(nv_i)}{\partial y}=0. \tag{9}$$

Components of gas phase read

$$\frac{\partial(\rho_1\phi_1 y_j)}{\partial t}+\frac{\partial(\rho_1\phi_1 y_j u_1)}{\partial x}+\frac{\partial(\rho_1\phi_1 y_j v_1)}{\partial y}=\omega_j. \tag{10}$$

The equation of state is

$$p=\rho RT\sum_1^m\frac{y_j}{w_j}. \tag{11}$$

In these equations, the subscripts 1, 2 and 2a denote the variables of gas, RDX and aluminum, respectively. The variables are as follows: ρ is the density, u is the lateral velocity, v is the longitudinal velocity, e is the internal energy, p is the pressure, ϕ ($\phi_1+\phi_2+\phi_{2\mathrm{a}}=1$) is the volume fraction of gas and particles. There are six components in gas, which are O_2, N_2, CO, CO_2, H_2O and Al(g). The reaction of $CO+0.5O_2\rightleftharpoons CO_2$ is also taken into account.[11] The mass production rate was given in Ref. [11]. Here y is the concentration, w is the molecular weight, and I is the interphase mass transfer. For the RDX, we use the model of Hong *et al.*[1] as follows:

$$I_{\mathrm{d}2}=\begin{cases}0, & T_2<T_{\mathrm{m}},\\ Q_{\mathrm{d}2}/L, & T_2\geqslant T,\end{cases} \tag{12}$$

where T_{m} is the melting point of RDX, and L is the latent energy of RDX. The RDX particles are accelerated by drag force of gas flow behind the shock wave and heated by convective heat transfer between the gas and particles. It is assumed that the melt part of the RDX particles are stripped by gas flow and are decomposed to release energy.

For the aluminum particles, the reaction rate is obtained from Price,[18] and they are coated by aluminum oxide. The particles will be ignited as its temperature reaches the melting point of aluminum because of the fracture of the aluminum oxide,[19]

$$I_{\mathrm{d}2\mathrm{a}}=\begin{cases}0, & T_{2\mathrm{a}}<T_{\mathrm{ign}},\\ -N\rho_{2\mathrm{a}}4\pi r^2\frac{dr}{dt}, & T_{2\mathrm{a}}\geqslant T_{\mathrm{ign}},\end{cases} \tag{13}$$

$$\frac{1}{r}\frac{dr}{dt}=-\frac{1}{kd_0^m/\Phi^{0.9}}, \tag{14}$$

where N is the number of particles in per unit volume, R is the radius of particle, $T_{\mathrm{ign}}=931\,\mathrm{K}$,[2] d_0 is the initial diameter of aluminum particles, Φ is the fraction of O_2, and m equals to 1.75.

Here F is the interphase drag force[20]

$$F_{\mathrm{d}ix}=\frac{n\pi R^2C_{\mathrm{d}}\rho_1\sqrt{(u_1-u_i)^2+(v_1-v_i)^2}(u_1-u_i)}{2}, \tag{15}$$

$$F_{\mathrm{d}iy}=\frac{n\pi R^2C_{\mathrm{d}}\rho_1\sqrt{(u_1-u_i)^2+(v_1-v_i)^2}(v_1-v_i)}{2}, \tag{16}$$

$$C_{\mathrm{d}}=\begin{cases}\frac{24(1+\frac{\mathrm{Re}^{\frac{2}{3}}}{6})}{\mathrm{Re}}, & \mathrm{Re}<1000,\\ 0.44, & \mathrm{Re}\geqslant 1000,\end{cases} \tag{17}$$

where C_{d} is the drag coefficient, and Re is the Reynolds number.

The interphase heat transfer Q is[17]

$$Q_{\mathrm{d}}=4n\pi R^2\lambda_1\mathrm{Nu}(T_1-T_2)/(2R), \tag{18}$$

where λ_1 is the heat conduct coefficient,[21] Nu is the Nusselt number, $\mathrm{Nu}=2+0.459\mathrm{Re}^{0.55}\mathrm{Pr}^{0.33}$, Pr is the Prandtl number, and q is the energy release of per unit mass of solid particles.[11]

To validate the numerical method, the Sod problem, the RDX dust and the aluminum dust detonation are simulated separately.

Sod:

$$t=0,$$
$$(\rho,u,p)=\begin{cases}(1,0.75,2.78), & 0<x<0.33,\\ (0.125,0,0.25), & 0.33<x<1,\end{cases}$$
$$\gamma=1.4.$$

The grid number is 200. From Fig. 1 it can be seen that the simulation agrees well with the Riemann Solution. The code can simulate the shock wave very well.

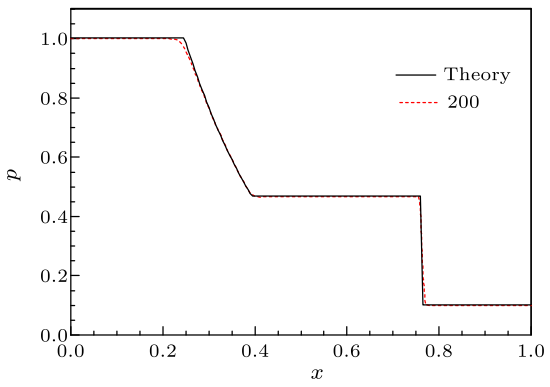

Fig. 1. The pressure of Sod's shock tube at $t=0.2$.

For the RDX dust, the concentration is $0.75\,\mathrm{kg/m^3}$ and the radius of particles is $20\,\mu\mathrm{m}$. The ignition conditions on the left are $\phi_1=1$, $\rho_1=3\,\mathrm{kg/m^3}$, $u_1=1000\,\mathrm{m/s}$, and $T_1=3600\,\mathrm{K}$. The wall boundary condition on the left, outflow boundary condition on the top and bottom and outflow boundary condition

on the right are applied. The velocity of the detonation is 1.899 km/s and the peak pressure is 4.75 MPa. The peak pressure is 4.84 MPa by the simulation of Eidelman and Yang.[22]

For the aluminum dust, the concentration is 0.304 kg/m^3 and the radius of particles is 1.7 μm. The initiation condition is the same as the above. The wall boundary condition on the left, top, bottom and the outflow boundary condition on the right are applied. The parameters of the detonation wave at 3.35 m are $D = 1.645$ km/s, $\rho_{CJ} = 2.21$ kg/m^3, $u_{CJ} = 564$ m/s, $p_{CJ} = 1.85$ MPa, $p = 3.41$ MPa. In the experiment of Tulis and Selman[23] the speed is 1.65 km/s. Detonation velocity by numerical simulation agrees well with that by experiment.

The density of RDX particles in the mixed dust is 0.565 kg/m^3 and the density of aluminum particles is 0.145 kg/m^3. The simulation area is 30 m × 0.2 m. The grid size is 5 mm. The initiation condition and boundary conditions are the same as that of the numerical simulation in single RDX dust detonation.

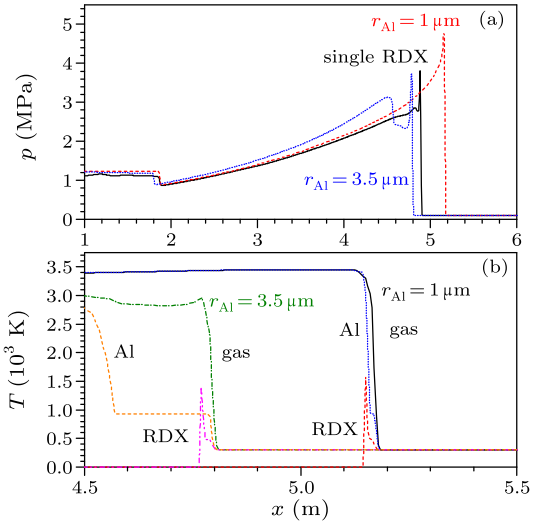

Fig. 2. Pressure (a) and temperature (b) at the same time with different Al radii.

For the radius of RDX particles of 10 μm, mixed dust detonation with different radii of aluminum particles is numerically simulated. Figure 2(a) is the pressure distribution of the mixed dust detonation. The lines from left to right stand for the single dust of RDX, mixed dust with $r_{Al} = 3.5$ μm, and the mixed dust with $r_{Al} = 1.0$ μm at the same time. Figure 2(b) is the temperature of gas, aluminum and RDX particles for $r_{Al} = 3.5$ μm and $r_{Al} = 1.0$ μm at the same moment. The left three lines stand for $r_{Al} = 3.5$ μm and the right stand for $r_{Al} = 1.0$ μm. From Fig. 2 we can see that as the radius of aluminum is 1 μm, the ignition times of aluminum particles are almost the same as those of RDX particles so that pressure of the detonation wave has only one peak. The pressure of the detonation is higher than that of single RDX dust detonation. As the radius of aluminum is 3.5 μm, ignition distance of aluminum particles is much longer than that of RDX particles, and the two peaks of pressure in detonation wave can be observed. Under this condition, double-front detonation is formed.

As the radius of aluminum particles becomes larger, the ignition time of particles will be longer. The mixed dust detonation of $r_{Al} = 4.0$ μm, $r_{RDX} = 10$ μm is simulated to analyze the steady state of the detonation wave. Figure 3 is the pressure distribution with interval of 1.428 ms after initiation in the model. From the results, it is found that the detonation wave becomes steady at 23 m and the velocity is 1.78 km/s. The second wave will run after the front wave, and the pressure of second wave is higher than that of the front wave. Under the influence of the second wave, the pressure of front wave also increases. The distance of the two waves is 0.15 m. The A point is the Chapman–Jouguet (CJ) point after the two waves.

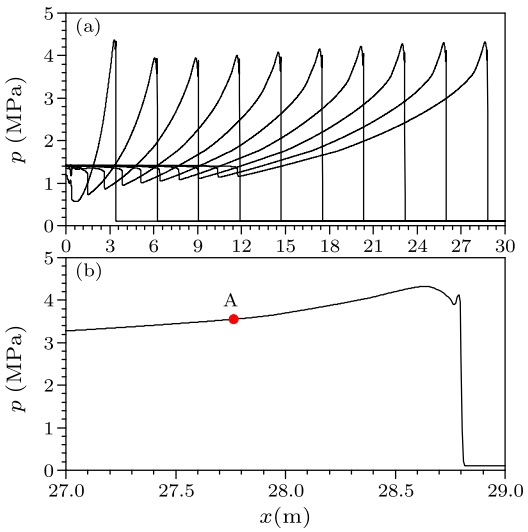

Fig. 3. Pressure (p (Pa)) distribution of $r_{Al} = 4.0$ μm, $r_{RDX} = 10$ μm.

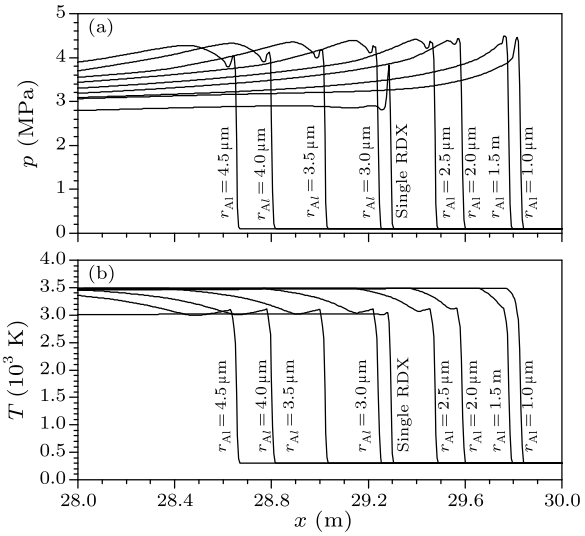

Fig. 4. Pressure (a) and temperature (b) of different models at 15.46 ms.

The curves in Fig. 4 from left to right are the pressure and temperature of single RDX for $r_{RDX} = 10$ μm and the mixed dust with the radius of aluminum particles of 4.5 μm, 4.0 μm, 3.5 μm, 3.0 μm, 2.5 μm, 2.0 μm, 1.5 μm and 1.0 μm. The detonation wave of $r_{Al} = 4.0$ μm, $r_{RDX} = 10$ μm is the latest to arrive at the steady state. From Fig. 3, it can be seen that the front waves of $r_{Al} = 4.0$ μm, $r_{RDX} = 10$ μm arrive

at the steady state after 23 m. As the radius of aluminum particles changes from 1.0 μm to 4.5 μm, the peak pressure of mixed dust detonation decreases and it is higher than that of single RDX dust detonation. As the radius of aluminum particles is larger than 2.0 μm, double-front detonation occurs. The ignition distance is longer as the aluminum particles become larger. However, the RDX particles release energy to form the first peak in very short distance. The ignition position of aluminum particles is far away from the ignition position of RDX particles, thus it has a small influence on the first peak. From Fig. 4(b) we can see that the temperature is higher behind the first peak as the radius of aluminum particles is smaller. Compared with the single RDX dust detonation, the pressure and temperature in the flow field of detonation of mixed dust are obviously higher.

Table 1 lists the parameters of mixed dust detonation wave with different radii of aluminum particles. The subscript f stands for the front wave, and b stands for the second wave. Because the grid size is larger that the distance from shock to the ignition point. The distance is achieved by interpolation. As the radius of aluminum particles is larger, the velocity, pressure and temperature of detonation wave will be slower. The pressure at the CJ point becomes lower as the radius of aluminum particles is larger. The peak pressure of the second wave is also lower. As the radius of aluminum particles is larger, the distance from shock to the ignition point of Al becomes larger and also the aluminum last at CJ point is more and the RDX is none. When the distance between the ignition point of Al and RDX becomes larger, the double-front detonation wave forms.

Table 1. Parameters of mixed dust detonation wave with different radii of aluminum particles. Here D is the velocity of detonation wave speed, $p_{\rm f}$ is the pressure of front wave, $p_{\rm b}$ is the pressure of second wave crest, $p_{\rm CJ}$ is the pressure of the CJ point, $T_{\rm CJ}$ is the temperature of the CJ point, $d_{\rm CJ}$ is the length of reaction area, $L_{\rm Al}$ is the distance from shock to the ignition point of Al, $L_{\rm RDX}$ is the distance from shock to the ignition point of RDX, and $fi_{\rm CJ}$ is the mass fraction of aluminum last at the CJ point.

$r_{\rm Al}$ (μm)	D (km/s)	$p_{\rm f}$ (MPa)	$p_{\rm b}$ (MPa)	$p_{\rm CJ}$ (MPa)	$T_{\rm CJ}$ (K)	$d_{\rm CJ}$ (m)	$L_{\rm Al}$ (mm)	$L_{\rm RDX}$ (mm)	$fi_{\rm CJ}$(%)
1	2.10	4.46		3.41	3435	0.45	2.3	2.3	0.7
1.5	1.98	4.45		3.30	3437	0.51	3.8	2.3	7.4
2	1.91	4.44	4.38	3.22	3428	0.56	7.4	2.9	24.07
2.5	1.88	4.34	4.41	3.15	3430	0.61	11.2	2.8	33.33
3	1.85	4.25	4.40	3.10	3478	0.75	14.9	2.9	55.93
3.5	1.82	4.17	4.35	3.05	3462	0.81	22.8	2.9	64.81
4	1.75	4.11	4.32	3.01	3475	0.84	30.0	3.0	67.78
4.5	1.76	4.05	4.27	2.99	3481	1.03	40.3	3.1	75.93

In summary, the detonation of mixed RDX and aluminum dust in air has been numerically simulated with the CE/SE method. For mixed dusts the density of RDX is 0.565 kg/m^3 and the density of aluminum is 0.145 kg/m^3. After increasing the simulation area, the result shows that the front detonation wave will arrive at a steady state very soon, but the second wave will increase continually. The second wave runs after the front wave, and the distance between the two waves becomes much smaller. The pressure of the front wave will also increase. For $r_{\rm Al} = 4.0$ μm, $r_{\rm RDX} = 10$ μm, the second wave will be stable at 23 m. For a fixed radius of RDX with 10 μm, double-front detonation appears as the radius of aluminum particles is larger than 2.0 μm because the distance between the ignition point of Al and RDX becomes larger. As the radius of aluminum particles increases from 1.0 μm to 4.5 μm, the peak pressure of mixed dust detonation decreases, and the second peak pressure changes slightly. The velocity of the detonation wave decreases from 2.1 km/s to 1.76 km/s. Comparing the detonation with single RDX dust, the pressure and temperature in the flow field of detonation of mixed dust are higher. The velocity of the detonation wave is larger when the radius of aluminum is below 3.0 μm.

References

[1] Hong T, Lin W Z and Qin C S 2010 *Chin. J. High Press. Phys.* **24** 15 (in Chinese)
[2] Hong T and Qin C S 2004 *Chin. J. Energ. Mater.* **12** 129 (in Chinese)
[3] Veyssiere B, Khasainov B A and Briand A 2008 *Shock Waves* **18** 307
[4] Briand A et al 2010 *Shock Waves* **20** 521
[5] Teng H H and Jiang Z L 2015 *The 29th International Symposium on Shock Waves* (Switzerland 2015) p 247
[6] Veyssiere B and Khasainov B A 1995 *Shock Waves* **4** 171
[7] Khasainov B A and Veyssiere B 1996 *Shock Waves* **6** 9
[8] Uphoff U and Hanel D 1996 *Shock Waves* **6** 17
[9] Michael C 1998 *The 11th International Detonation Symposium* (Colorado 1998) p 193
[10] Khasainov B A and Ermolaev B S 2002 *The 12th International Detonation Symposium* (California 2002) p 501
[11] Hong T et al 2009 *Expl. Shock Wave* **29** 468 (in Chinese)
[12] Chang S C 1995 *J. Comput. Phys.* **119** 295
[13] Zhang D L and Wang J T 2009 *Chin. J. Comput. Phys.* **26** 211
[14] Wang J T et al 2007 *Chin. J. Comput. Phys.* **24** 395
[15] Wang G et al 2010 *Chin. Phys. Lett.* **27** 024701
[16] Dong H F et al 2011 *Chin. Phys. Lett.* **28** 030203
[17] Liu D Y 1993 *Fluid Dynamics of Two-Phase Systems* (Beijing: Higher Education Press) (in Chinese)
[18] Price E W 1984 *Progress in Astronautics and Aeronautics: Fundamentals of Solid-Propellant Combustion* (New York 1984) p 479
[19] Hong T and Qin C S 2003 *Expl. Shock Wave* **23** 295 (in Chinese)
[20] Sehliehting H 1983 *Boudary Layer Theory* (New York: McGraw-Hill)
[21] Yang S M and Tao W S 2006 *Heat Transfer Theory* (Beijing: Higher Education Press) (in Chinese)
[22] Eidelman S and Yang X L 1993 *Combust Sci. Tech.* **89** 201
[23] Tulis A J and Selman J R 1982 *The 19th International Symposium on Combustion* (The Combustion Institute 1982) p 655